How structural brain network topologies associate with cognitive abilities in a value-based decision-making task

Cristina Bañuelos[1,2], Timothy Verstynen, Ph.D.[2,3,4]
[1]*Dept. Biological Sciences, Carnegie Mellon University, Pittsburgh, Pennsylvania 15213*
[2]*Dept. Psychology, Carnegie Mellon University, Pittsburgh, Pennsylvania 15213*
[3]*Carnegie Mellon Neuroscience Institute, Carnegie Mellon University, Pittsburgh, Pennsylvania 15213*
[4]*Dept. Biomedical Engineering, Carnegie Mellon University, Pittsburgh, Pennsylvania 15213*

Value-based decision-making relies on effective communication across disparate brain networks. Given the scale of the networks involved in adaptive decision-making, variability in how they communicate should impact behavior; however, precisely how the topological pattern of structural connectivity of individual brain networks influences individual differences in value-based decision-making remains unclear. Using diffusion magnetic resonance imaging, we measured structural connectivity networks in a sample of community dwelling adults (N = 124). We used standard graph theoretic measures to characterize the topology of the networks in each individual and correlated individual differences in these topology measures with differences in the Iowa Gambling Task. A principal components regression approach revealed that individual differences in brain network topology associate with differences in both optimal decision-making, as well as in each participant's sensitivity to high frequency rewards. These findings show that aspects of structural brain network organization, specifically small-world style topologies, can determine the efficiency with which information is used in value-based decision-making.

Abbreviations: MRI - Magnetic Resonance Imaging; IGT – Iowa Gambling Task; DWI – Diffusion Weighted Imaging; QSDR – Q-Space Diffeomorphic Reconstruction; PCA – Principal Components Analysis; GLM – Generalized Linear Models

Keywords: Value-based decision-making; Adaptive decision-making; Decision-making; Iowa Gambling Task; Graph-theoretic Topology; Structural brain networks

Introduction

The human brain consists of 86 billion interconnected neurons that form a series of interconnected & hierarchically organized networks (Herculano-Houzel, 2009). There are input-output computations made across all regions of the brain, connected by bundles of axon fibers that communicate across long distances (Hopfield, 1982; Mountcastle, 1997). Fast and efficient communication throughout the brain is necessary for nearly all cognitive processes. This highly complex series of networks is organized through cell bodies, dendrites, and axon terminals of these neurons that, together, make up the "grey matter," whereas the axons connecting the cell bodies to the axon terminals make up the "white matter." From a graph theoretical perspective, grey matter reflects the nodes that process information, and white matter forms the edges that determine which information is sent between nodes. The exact nature of the wiring architecture of the human brain, much like a circuit in a computer,

impacts brain function and leads to subsequent cognition (McCulloch, 1944; Johansen-Berg, 2010; Hermundstad et al., 2014). The static organization of the structural architecture of the brain is both modular and hierarchical, supporting the execution of local operations and global integration of segregated functions (Park & Friston, 2013). Being able to measure the individual differences in structural connectivity of brain networks and their behavior would further explain the neural constraints on complex cognition (Verstynen, 2015).

The structural connectivity of brain networks is measured through a technique known as diffusion-weighted imaging (DWI). DWI takes advantage of the diffusion properties of water molecules within the axons of the myelinated white matter fascicles. Diffusion tensor imaging is one of the most popular DWI sampling schemes. It samples a few dozen orthogonal diffusion directions that are used to calculate a tensor of average diffusion direction within each volumetric pixel (i.e., "voxel", the fundamental unit of the 3-dimensional brain images) (for review, see Vettel et al., 2017). DWI has been used in conjunction with graph theoretic structural topology measures in order to understand the functional organization underlying structural networks (for review see Bullmore & Sporns, 2009).

There is a growing body of evidence that brain networks have small-worldness properties. These properties can be characterized as a dense local clustering between neighboring nodes forming modules, or distinct functional areas, paired with short path length between any pairs between modules (Watts & Strogatz, 1998). Small-worldness can be thought of as the measure of how interconnected neighboring nodes are without inefficiently being connected to more distant nodes, forming hubs or "small worlds." This small-worldness supports the distributed nature of distinct brain areas while also demonstrating how these modules are integrated into global brain networks (Bassett & Bullmore 2006). However, we still have a limited understanding of how the topological organization of structural connections in the brain predicts individual differences in complex cognitive abilities.

To gain insights into how the brain may be organized to carry out executive processes, we looked into how the structural network organization may explain differences in executive abilities that are necessary to complete complex cognitive tasks. Specifically we thought that executive processes would be sensitive to network organization because they require efficient communication across disparate brain regions, from sensory processing to abstract task representations. Using DWI methods, we measured whether individual differences in white matter topology, as seen through graph theoretic measures, associate with value-based decision-making (payoff or sensitivity to frequency of reward). Value-based decision-making is a complex task that, at a minimum, uses visual perception, attention, working memory, reinforcement learning, executive control, and other lower order functions in order to synthesize our decisions, and therefore relies on the efficient communication across global brain networks (Bechara et al., 1994). Positing that small-worldness is a property of efficient network communication, then we hypothesize that individuals with more small world structural networks would be better at feedback driven, value-based decision-making.

Materials and Methods

Participant Characteristics

We used an already collected sample of community dwelling adults in Pittsburgh taken from the Weight-loss Intervention for brain Networks (WIN) project and collected at the University of Pittsburgh and Carnegie Mellon

University. The sample consisted of 124 participants (97 females, 27 males) between the ages of 22 and 55 (M= 44.38 years, SD=8.49). The participants had between 9 and 25 years of education (M= 16 years, SD=2.67). These participants were part of a larger project that included the completion of many other tasks, some of which were completed within the magnetic resonance imaging (MRI) scanner. This research project was approved by the institutional review boards at both the University of Pittsburgh and Carnegie Mellon University.

Iowa Gambling Task

While in the MRI scanner, participants completed a computerized version of the Iowa Gambling Task (IGT). The IGT is a popular task for assessing decision-making and executive function in healthy and clinical populations (Buelow & Suhr, 2009). While popular, we do acknowledge that the test retest reliability of the IGT has come under scrutiny, and critical issues have arisen regarding construct validity. Nonetheless experimental evidence continues to provide support of the IGT in detecting decision-making deficits in both healthy and clinical populations (Buelow & Suhr, 2009).

In the IGT, participants are asked to select a card from any of the four decks presented with a varying amount of reward or punishment (Figure 1; Bechara et al., 1994). The participants specifically select one card at a time from any of the 4 decks for a total of 100 card selections. The participants are given a loan of $2000 and were instructed that the goal of the task is to maximize profit. They are also allowed to switch between any of the decks at any time and as often as they wished. The participants were not aware of any of the deck specifications and were only informed that each deck was different (Table 1). With each selection from Decks A or B (the "disadvantageous decks"), participants have a net loss of money. With each selection from Decks C or D (the "advantageous decks"), participants have a net gain of money. The amount of reward or punishment varied between decks and the position within a deck. Deck A and Deck B both had the same amount of overall net loss. However, in Deck A the reward was less frequent and higher in magnitude, while in Deck B the reward was more frequent and higher in magnitude. Similarly, Deck C and Deck D had the same overall net gain. In Deck C the reward was less frequent and lower in magnitude, while in Deck D the reward was more frequent and higher in magnitude. From the selections made by the participants, their overall payoff (P = (C + D) - (A + B)) and their overall sensitivity to frequency of reward (Q = (B + D) - (A + C)) was calculated.

	A	B	C	D
Reward	$100	$100	$50	$50
Frequency of Reward	Low	High	Low	High
Net Yield	Loss	Loss	Gain	Gain

Table 1: Iowa Gambling Task Deck Specifications. The decks have a different combination of two separate features including reward amount, frequency of reward, and result in either a net yield of overall loss or gain.

Figure 1: Computerized version of the Iowa Gambling Task. The computerized version of the IGT that participants were asked to complete is shown above. They were asked to select a card from any of the four decks presented with a varying amount of reward or punishment. The amount of cash earned and lost is shown in the green and red values, respectively.

Diffusion Weighted Imaging

All diffusion weighted images were acquired using a single-shell, diffusion tensor

imaging protocol (voxel size = 2.4×2.4×2.4 mm, TR = 11100 ms, TE = 96 ms, 56 different directions, b-value = 2000 s/mm^2) on a 3-Tesla Verio Prisma MRI system. DWI data was reconstructed using a q-space diffeomorphic reconstruction (QSDR) method. This creates models of water diffusion patterns for every voxel in the brain in an averaged space that allows for comparison across participants (Yeh & Tseng, 2011). A deterministic fiber tractography approach (Yeh et al., 2013) was then used to estimate the structural connections between brain areas for each participant (left in Figure 2), using standard tractography parameters (anisotropy threshold = 0.70, random seed orientation, tracked streamline count = 250,000, step size = 1mm, max turning angle = 75 degrees, smoothing = 0.50, minimum length = 20mm, maximum length = 160mm). The fiber tractography output was integrated with a gray matter brain atlas, using a well-established parcellation of distinct regions known as nodes (middle in Figure 2) to produce a connectivity matrix (right in Figure 2).

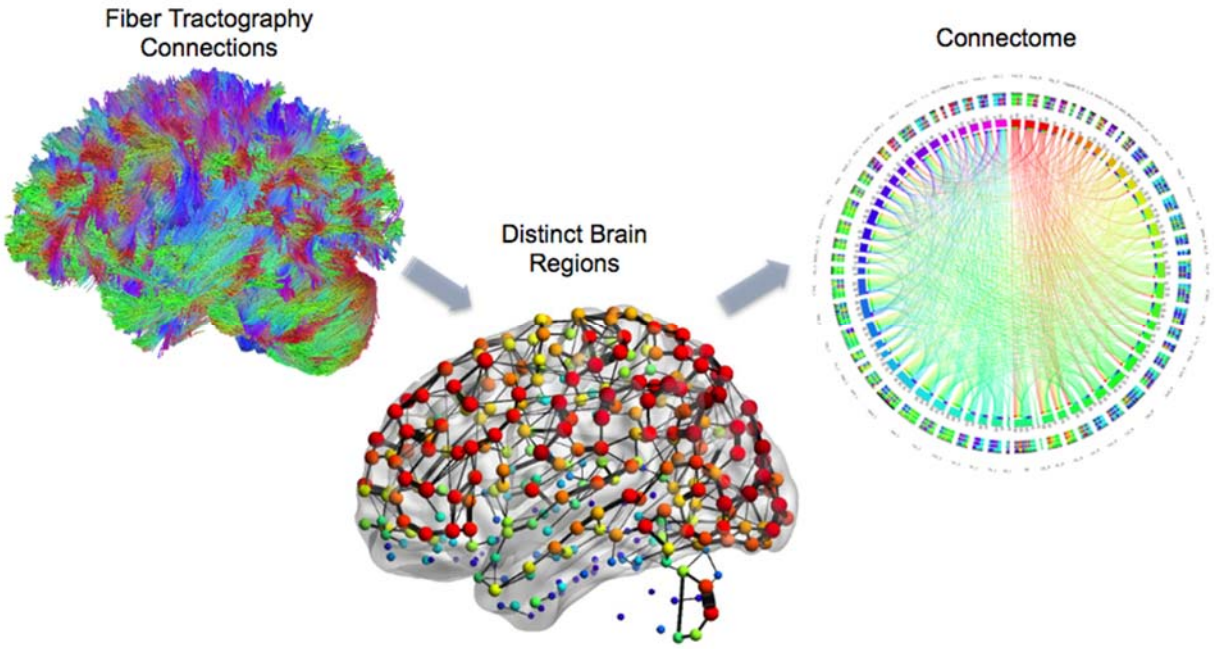

Figure 2: Brain Network Connectome. The fiber tractography DWI structural connections are used as the edges. They are then added to gray matter that is parcellated into distinct regions with a brain atlas to form the brain topologies. Together they form a brain graph representation of a brain network, and can be plotted as a connectome.

Brain Network Connectivity Mapping

Brain networks can be defined through connectivity matrices made of rows and columns for each node in the network, while the values represent the connections between each pair of nodes. The weight of edges in the matrix were defined by the number of streamlines connecting each pair of nodes (Tang et al., 2017). The analyses were also replicated using a different definition for edge weights in which they were equal to the number of individual white matter tracts connecting each pair of nodes divided by the total volume of the node pair. The network system was represented by a graph consisting of (n, e), where n referred to the node (grey matter regions of interest), and e referred to the set of all edges on the graph. Each node was assigned a real value. The node states present under one gray matter region were used to define the map. The

structural topology measures (Figure 3) on each subject's connectivity matrix include:

- ***Density:*** the fraction of present connections to all possible connections without taking into account any connection weights in the calculation (Rubinov & Sporns 2010)
- ***Clustering Coefficient:*** the fraction of triangles (3 nodes and 3 edges that connected together form a triangle) around a node (Rubinov & Sporns 2010)
- ***Transitivity:*** the ratio of triangles to triplets (3 nodes and 2 edges that are connected in series) in the network, which can be used as an alternative measure to the clustering coefficient (Rubinov & Sporns 2010), although these are not identical metrics
- ***Characteristic Path Length:*** the average shortest path length in the network (Rubinov & Sporns)
- ***Small-worldness:*** dense local clustering or cliquishness of connections between neighboring nodes yet a short path length between any (distant) pair of nodes due to the existence of relatively few long-range connections (Bassett & Bullmore 2006)
- ***Global Efficiency:*** the average inverse shortest path length in the network (Rubinov & Sporns 2010)
- ***Local Efficiency:*** the global efficiency computed on node neighborhoods, and is related to the clustering coefficient (Rubinov & Sporns 2010)
- ***Assortativity Coefficient:*** a correlation coefficient between the degrees of all nodes on two opposite ends of a link, where a positive value would indicate that nodes tend to link to other nodes with the same or a similar degree (Rubinov & Sporns 2010).

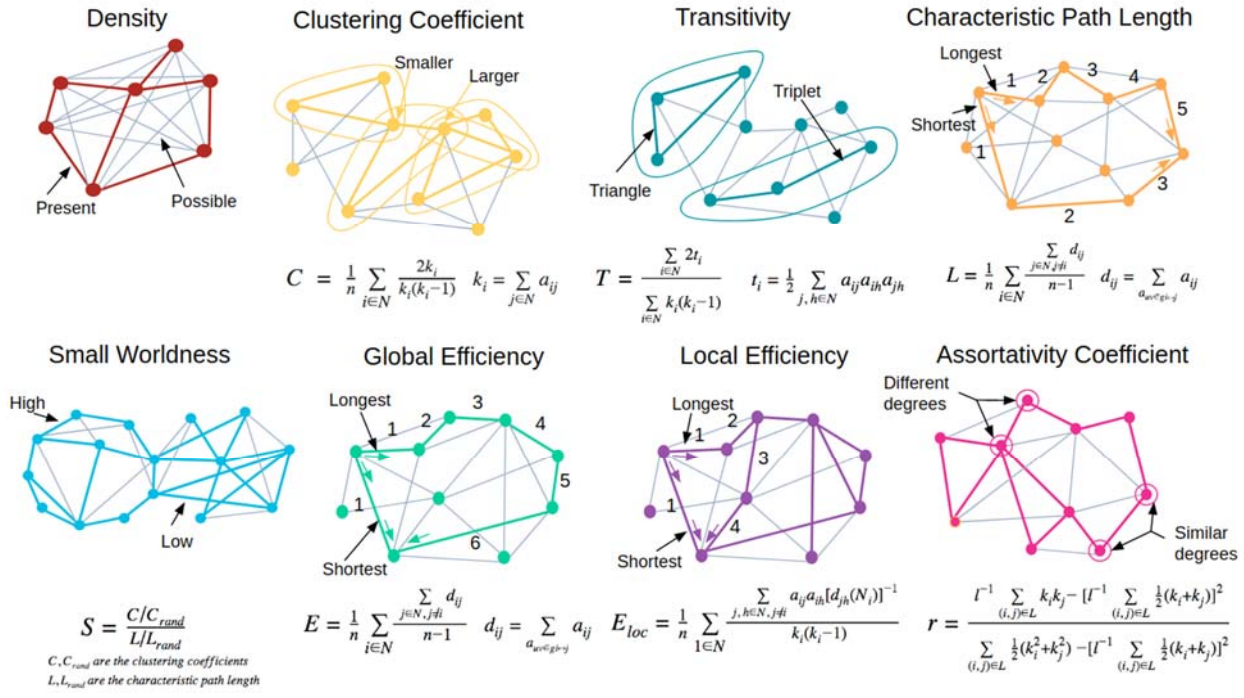

Figure 3: Graphed Structural Topology Measures. For each subject we looked at 8 measures of structural network topology, related to the "small worldness" of the brain networks (Rubinov & Sporns 2010; Bassett & Bullmore 2006). The measures included Density, Clustering Coefficient, Transitivity, Characteristic Path Length, Small Worldness, Global Efficiency, Local Efficiency, and Assortativity Coefficient.

	Minimum	Quartile.1	Median	Mean	Quartile.3	Maximum	Skew	Outliers
Density	0.042	0.052	0.055	0.055	0.058	0.07	0.027	1
Clustering Coefficient	0.128	0.226	0.253	0.253	0.277	0.389	0.113	1
Transitivity	0.005	0.023	0.036	0.039	0.053	0.128	1.074	1
Net. Char. Path Length	2.979	3.331	3.455	3.516	3.682	4.582	1.238	1
Small Worldness	0.036	0.063	0.072	0.072	0.081	0.106	0.011	1
Global Efficiency	0.296	0.337	0.349	0.348	0.36	0.396	-0.359	1
Local Efficiency	9.367	16.878	18.656	18.67	20.631	28.049	0.078	1
Assortativity	-0.308	-0.162	-0.085	-0.079	0.008	0.191	0.15	1
P Scores	-54	0	23	21.831	46	70	-0.229	1
Q Scores	-60	14	38	31.331	52.5	84	-0.774	1

Table 2: Distribution of Measures. The distribution measures of the structural topology measures and IGT scores calculated are minimum, quartile 1, median, quartile 3, maximum, skew, and the number of Grubbs test outliers.

Results

Characteristics and Distribution of Measures

The distribution of structural network topology measures and the IGT scores are reported as minimum, quartile 1, median, quartile 3, maximum, skew, and number of Grubbs test outliers (Table 2). The Grubbs test outliers were calculated with an alpha level of 0.05. Transitivity, Characteristic Path Length, and Q-Scores have the greatest magnitude of skewness calculated with 1.074, 1.238, and -0.780, respectively. With the Grubbs test for calculating outliers, all of the variables had a single outlier.

When looking across the network topology measures, there was a high degree of correlation across individuals, measured using Pearson's correlation coefficient (Figure 4). The greatest positive correlations observed were between Small Worldness and Local Efficiency with 0.88, Clustering Coefficient and Small Worldness with 0.90, and Clustering Coefficient and Local Efficiency with 0.97. Such strong correlations among the structural topology measures suggest that they share the common variance. High correlations among variables provide evidence of a low dimensional structure in the topology measures.

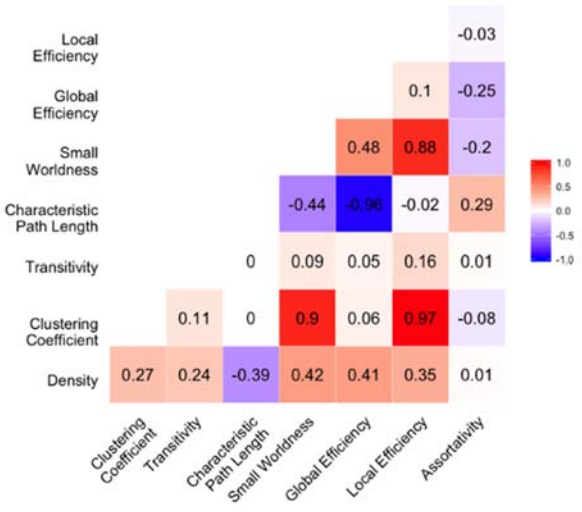

Figure 4: Correlation matrix of the structural topology measures. Strong negative correlations are depicted as blue, zero correlations are depicted as white, and strong positive correlations are depicted as red. Characteristic Path Length and Global Efficiency were found to have a strong negative correlation. Strong positive correlations were found between Small Worldness and Local Efficiency, Clustering Coefficient and Small Worldness, and Clustering Coefficient and Local Efficiency.

Since strong correlations were observed among the network topology measures in the data, Principal Component Analysis (PCA) was

used to identify the lower dimensional components that explain most of the variance in these measures. PCA orthogonally transforms the highly correlated data into linearly uncorrelated

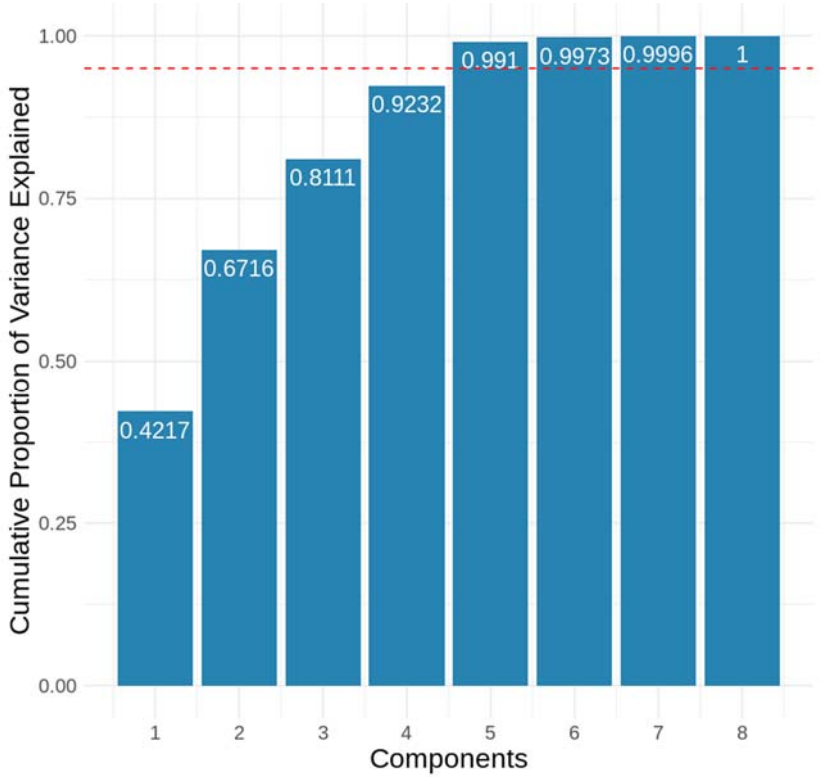

Figure 5: Principal Components for 95% Variance Explained. The cumulative proportion variance for each of the 8 PCA components are plotted in the blue bars. The red dotted line demonstrates the mark for 95% of cumulative proportion of variance. The barplot shows that components 1 through 5 account for over 95% of the cumulative proportion variance. Components 1-5 have a cumulative proportion variance that is about equal to 99.10%.

Components	1	2	3	4	5	6	7	8
Density	-0.324	0.129	-0.473	-0.167	0.789	-0.015	-0.054	0.013
Clustering Coefficient	-0.435	-0.405	0.148	0.001	-0.062	-0.212	-0.336	0.68
Transitivity	-0.111	-0.063	-0.702	0.618	-0.327	-0.046	-0.013	-0.008
Characteristic Path Length	0.302	-0.565	-0.021	0.111	0.209	0.527	-0.469	-0.187
Small Worldness	-0.525	-0.114	0.146	-0.05	-0.135	-0.285	-0.322	-0.696
Global Efficiency	-0.33	0.529	-0.015	-0.122	-0.269	0.633	-0.333	0.115
Local Efficiency	-0.447	-0.389	0.056	-0.03	-0.037	0.436	0.67	-0.067
Assortativity	0.132	-0.229	-0.487	-0.748	-0.361	-0.059	-0.02	-0.007

Table 4: Table of PCA Component Loadings for Variables. Component 2 has 7 variables with significant loadings, and it has a strong positive loading with Global Efficiency, and strong negative loadings on Characteristic Path Length, Clustering Coefficient, and Local Efficiency. Component 5 has 6 variables with significant loadings, and it has a strong positive loading on Density, and strong negative loadings on Transitivity and Assortativity.

principal components. PCA has the ability to reduce the dimensionality of data while maintaining useful information.

Table 4 shows the recovered 8 components and their mapping to the variables measured. Loadings were considered to be significant when they had a magnitude greater than 0.1, and strong when they had a magnitude greater than 0.3. In the first PCA component, all of the 8 variables measured are significantly loaded. There are strong positive loadings with Density, Clustering Coefficient, Small Worldness, and Local Efficiency, and there is a strong negative loading on Characteristic Path Length. Component 2 has significant loadings from 7 components. There is a strong positive loading on Global Efficiency, and there are strong negative loadings on Clustering Coefficient, Characteristic Path Length, and Local Efficiency. Component 3 has 5 variables with significant loadings. There is strong positive loadings on Density, Transitivity, and Assortativity, and there are no strong negative loadings. Component 4 has 5 variables with significant loadings. There is a strong positive loading on Assortativity, and there is a strong negative loading on Transitivity. Component 5 has 6 variables with significant loadings. There is a strong positive loading on Density, and there are strong negative loadings on Transitivity and Assortativity. Component 6 has 5 variables with significant loadings. There are no strong positive loadings, and there are strong negative loadings on Characteristic Path Length, Global Efficiency, and Local Efficiency. Component 7 has 5 variables with significant loadings. The strong positive loadings are on Clustering Coefficient, Characteristic Path Length, Small Worldness, and Global Efficiency, and the strong negative loading is on Local Efficiency. Component 8 has 4 variables with significant loadings. There is a strong positive loading on Clustering Coefficient, and there is a strong negative loading on Small Worldness.

When looking at the percent variance accounted for (Figure 5), we found that only the first 5 components explained 95% of the data. Therefore our subsequent analysis only focuses on these components.

Associations with IGT Performance

A generalized linear model (GLM) was used to identify which of the 5 principal components that explained the most variance were associated with the P and Q-Scores of the participants. A significant association between Component 2 and the P-Score was found, which reflects the ability to effectively use feedback to maximize returns, with a significance level of less than 0.1 (Table 5). The GLM with the P-Scores and the first 5 principal components predicts P-Scores with a correlation of 0.232. The rest of the components do not appear to be able to predict P-Scores accurately with a significance level of less than 0.1. Component 2 was found to have mean bootstrap coefficient estimate of 3.05 and a lower and upper bound of 2.735 and 3.365 (Table 9).

Components 1, 2, 3, and 5 were found to have positive coefficient estimates with standard errors ranging from 1.37 to 3.42 (Table 5). Component 4 was found to have a negative coefficient estimate with a standard error of 1.77 (Table 5). Component 2, with a coefficient estimate of 3.07 and a standard error of 1.77, was the only component found to predict P-Scores with a significance level of $p = 0.088$ (Table 5). The intercept was found to have a coefficient estimate of 21.83 and a standard error of 2.51 with a significance of $p < 0.001$ (Table 5). This is lower than the Bonferroni corrected threshold of 0.005 (corrected for 10 comparisons). The cross validation errors calculated from the GLM are 1.06 and 1.06, which are significantly low values. The rest of the components do not appear to be able to predict P-Scores as they had significance levels of $p > 0.1$ (Table 5).

	Coefficient Estimates (Std. Error)
Intercept	21.831 (2.517)***
Component 1	-1.72 (1.37)
Component 2	3.065 (1.78) .
Component 3	-0.986 (2.383)
Component 4	2.363 (2.657)
Component 5	3.066 (3.418)

Significant codes: *** = 0.001, ** = 0.01, * = 0.05, . = 0.1

Table 5: GLM Analysis on Principal Components to Predict P-Score. The generalized linear model to predict P-Scores with the PCA components shows that the second component was able to reliably predict P-Scores with a significance of $p < 0.1$.

A significant association between the Component 5 and the Q-Score was found, which reflects a sensitivity to high frequency rewards (Table 6) with a significance of $p < 0.05$. The GLM with the Q-Scores and the first 5 principal components predicts Q-Scores with a correlation of 0.318. The rest of the components do not appear to be able to predict Q-Scores with a significance level of less than 0.1. Component 5 was found to have a mean bootstrap coefficient estimate of 7.579 and a lower and upper bound of 6.7 and 8.065 (Table 9).

Components 2, 4, and 5 were found to have positive coefficient estimates with standard errors ranging from 1.41 to 3.52 (Table 6). Components 1 and 3 were found to have negative coefficient estimates with standard errors of 1.41 and 2.46, respectively (Table 6). Component 5, with a coefficient estimate of 7.46 and a standard error of 3.52, was the only component found to predict Q-Scores with a significance level of $p = 0.034$ (Table 6). The intercept was found to have a coefficient estimate of 31.44 and a standard error of 2.59 with a significance of $p < 0.001$ (Table 6). This is lower than the Bonferroni corrected threshold of 0.005 (corrected for 10 comparisons). The cross validation errors calculated from the GLM are 1.06 and 1.06, which are significantly low values. The rest of the components do not appear to be able to predict Q-Scores as they had significance levels of $p > 0.1$ (Table 5).

	Coefficient Estimates (Std. Error)
Intercept	31.331 (2.594)***
Component 1	0.773 (1.412)
Component 2	2.249 (1.835)
Component 3	3.484 (2.456)
Component 4	-2.908 (2.739)
Component 5	7.579 (3.523)*

Significant codes: *** = 0.001, ** = 0.01, * = 0.05, . = 0.1

Table 6: GLM Analysis on Principal Components to Predict Q-Score. Component 5 with a coefficient estimate of 7.46 and standard error of 3.52 was the only Component found to can predict Q-Scores with a significance of 0.01. The rest of the components do not appear to be able to predict Q-Scores with a significance level of less than 0.01.

Using only the Component 2 model coefficients as weights for each component in predicting P-Scores the value of the weights from the components can be transformed into data space with the topology measures. Their data space transformation demonstrates that Global Efficiency leads to an increase in P-Score, whereas Characteristic Path Length, Clustering Coefficient, Global Efficiency, Local Efficiency, and Assortativity lead to a decrease in P-Score. Global Efficiency has the greatest positive effect on P-Scores, and Characteristic Path Length has the greatest negative effect (Table 7).

Using only the Component 5 model coefficients as weights for each component in predicting Q-Scores, the value of the weights from the components can be transformed into data space with the topology measures. Their data space transformation demonstrates that Density and Characteristic Path Length lead to an increase in Q-Score, whereas Clustering Coefficient, Transitivity, Small Worldness, Global Efficiency, Local Efficiency, and Assortativity lead to a decrease in Q-Score (Table 8). Density has the greatest positive effect on Q-Scores and transitivity has the greatest negative effect.

	Weight	SE of Weight	Lower Bound	Upper Bound
Density	0.396	0.23	-0.055	0.847
Clustering Coefficient	-1.242	0.721	-2.656	0.172
Transitivity	-0.192	0.112	-0.411	0.027
Characteristic Path Length	-1.732	1.006	-3.703	0.239
Small Worldness	-0.348	0.202	-0.744	0.048
Global Efficiency	1.62	0.941	-0.224	3.464
Local Efficiency	-1.192	0.692	-2.549	0.165
Assortativity	-0.701	0.407	-1.5	0.097

Table 7: Structural Topology Weights of Component 2 in Topology Space. In topology space, Component 2 was made up of primarily Characteristic Path Length, Global Efficiency, Local Efficiency, Transitivity, Clustering Coefficient, and Assortativity.

	Weight	SE of Weight	Lower Bound	Upper Bound
Density	5.9827	2.7808	0.5323	11.433
Clustering Coefficient	-0.4699	0.2184	-0.8981	-0.0418
Transitivity	-2.476	1.1509	-4.7316	-0.2203
Characteristic Path Length	1.5864	0.7374	0.1411	3.0316
Small Worldness	-1.0268	0.4773	-1.9623	-0.0914
Global Efficiency	-2.0363	0.9465	-3.8914	-0.1812
Local Efficiency	-0.2837	0.1319	-0.5422	-0.0252
Assortativity	-2.738	1.2726	-5.2323	-0.2436

Table 8: Structural Topology Weights of Component 5 in Topology Space. In topology space, Component 5 was made up of primarily Density, Transitivity, Global Efficiency, & Assortativity.

	Component Estimate	Mean Bootstrap	Standard Deviation	Error	Lower Bound	Upper Bound
Component 2 with P-Score	3.065	3.006	1.795	-0.316	2.691	3.322
Component 5 with Q-Score	7.579	7.103	4.081	-0.718	6.384	7.821

Table 9: Bootstrapping Analysis on Principal Components with P and Q-Scores. Component 2 with P Score was found to have a mean bootstrap coefficient estimate of 3.05, whereas Component 5 with Q-Score was found to have a mean bootstrap coefficient estimate of 7.579.

Discussion

In this experiment we found evidence that supports the hypothesis that individuals with more small-world structural brain networks would be better at feedback driven value-based decision-making. First, the graph topology measures of white matter networks had a low dimensional structure that could be mostly explained by five principal components. A regression analysis examining how these components correlated with the ability to use

feedback to maximize long-term payoffs (P-Score) and the sensitivity to high frequency rewards (Q-Score) found associations with both. Only Component 2, that had strong positive loadings on Global Efficiency, and strong negative weights on Characteristic Path Length and Local Efficiency, reliably associated with the ability to use feedback to maximize rewards (Table 7). The positive loadings associate with greater ability, and the negative loadings associate with lesser ability (Table 7). Another component, Component 5, which had strong positive loadings on Density and Characteristic Path Length, and strong negative loadings on Transitivity, Global Efficiency, and Assortativity, reliably associated with the sensitivity to rewards. The positive loadings associate with greater sensitivity, and negative weights associate with a lesser sensitivity (Table 8).

These results contribute to the mounting evidence that efficient network topologies, such as small-worldness, associate with efficient cognitive properties, further supporting the distributed nature of distinct brain areas while demonstrating the importance of integrated and efficient communication between these areas within global brain network (Bassett & Bullmore, 2006; Douw et al., 2011; Vlooswijk et al., 2011; Pandit et al., 2013). The efficient communication between global brain networks is especially important in higher order cognitive tasks such as value-based decision-making which uses, at a minimum, visual perception, attention, working memory, reinforcement learning, executive control, and other lower order functions in order to synthesize our decisions. The IGT is one such cognitively demanding task, requiring participants to select which deck they believe is of highest value and refine this value estimate of their actions using feedback from previous outcomes, in order to converge to an optimal decision. In this way, the IGT represents a complex multi-armed bandit task, as typically used in reinforcement learning (Sutton & Barto, 1998), but with dynamic reward structures.

The analysis reported here was strictly cross-sectional in nature. However, since the strength of connections in white matter networks is highly plastic (Yeh et al., 2016), a more optimal design may have been a longitudinal study in which individuals were tracked over time. Furthermore, node-wise topology measures were not looked at and primarily focused on using the topology measures of global networks. It could be that small differences in specific pathways, such as the cortico-basal ganglia thalamic loops (Alexander, DeLong, & Strick, 1986), are highly predictive of aspects of value-based decision-making, but by looking at global networks this effect is washed out.

Despite this limitation, the results reported here have provided further evidence for an underlying brain network architecture that constrains behavioral differences between individuals in value-based decision-making. A complete and thorough understanding of the structural topological pattern of human brain connectivity would allow one to understand optimal and suboptimal structural architectures in brain networks with regards to behavior. Furthermore, that could provide insights to behavioral pathologies, and could potentially lead to a new pathway for diagnosis of psychiatric and neurological pathologies with abnormal signatures of structural topological organization.

Future directions could include focusing on regions of interest or subnetworks of interest in order to identify individual network associations rather than global network associations. In addition, the functional dynamics of the global networks could be more sensitive to individual differences in decision-making. By looking at functional connectivity or task-linked responses instead of structural connectivity, may give rise to a complete understanding of the nature of the communication across these networks.

Future applications of this work include using the topological organization of the structural connectivity of brain networks as neuroimaging markers for different decision-types or other cognitive states. For example, a similar analysis on other complex decision tasks (e.g., the Stroop task) could be performed. In addition, future studies could be more strategic in the brain networks of interest. For example, future work could have a more detailed focus on regions of interest such as the basal ganglia pathways that play a critical role in reinforcement learning and decision-making. They could also integrate both structural and functional connectivity measures to provide a holistic understanding of the network form and function.

In summary, this study demonstrates how the architecture of white matter networks have a low dimensional structure in their topological organization, and how a subset of these low dimensional components reliably associated with individual differences in the ability to use feedback to modify future decisions. Specifically individuals with structural connections that allowed for more efficient long-range communication between brain areas were better at using feedback to maximize future long-term rewards.

Endnotes

The data and analysis steps can be accessed at: github.com/cbanuelos/Structural_Topology_Brain_Networks.

Acknowledgements

This research was supported through the mentorship of Timothy Verstynen, Ph.D., through the Cognitive Axon Lab at Carnegie Mellon University. We would also like to acknowledge the guidance from Alexis Porter, and Daniel Brasier, Ph.D in the completion of this research project. This work was funded by the National Institutes of Health R01 DK095172.

Corresponding Author

Cristina Bañuelos
Carnegie Mellon University
5000 Forbes Avenue,
Pittsburgh, PA, 15213
cbanuelo@andrew.cmu.edu

References

Alexander, G. E., DeLong, M. R., & Strick, P. L. (1986). Parallel organization of functionally segregated circuits linking basal ganglia and cortex. Annu Rev Neurosci 9:357-381.

Bassett, D. S., & Bullmore, E. D. (2006). Small-world brain networks. Neuroscientist 12: 512-523.

Bechara, A., Damasio, A. R., Damasio, H., & Anderson, S. W. (1994). Insensitivity to future consequences following damage to human prefrontal cortex. Cognition 50: 7-15.

Buelow, M. T., & Suhr, J. A. (2009). Construct validity of the Iowa gambling task. Neuropsychol Rev 19:102-114.

Bullmore, E., & Sporns, O. (2009). Complex brain networks: graph theoretical analysis of structural and functional systems. Nature Rev Neurosci 10:186.

Douw, L., Schoonheim, M. M., Landi, D., Van der Meer, M. L., Geurts, J. J. G., Reijneveld, J. C., ... & Stam, C. J. (2011). Cognition is related to resting-state small-world network topology: an magnetoencephalographic study. Neuroscience 175:169-177.

Herculano-Houzel, S. (2009). The human brain in numbers: a linearly scaled-up primate brain. Front Hum Neurosci 3:31.

Hermundstad, A. M., Brown, K. S., Bassett, D. S., Aminoff, E. M., Frithsen, A., Johnson, A., ... & Carlson, J. M. (2014). Structurally-

constrained relationships between cognitive states in the human brain. PLoS Comput Biol 10:e1003591.

Hopfield, J. J. (1982). Neural networks and physical systems with emergent collective computational abilities. Proc Natl Acad Sci 79:2554-2558.

Johansen-Berg H. (2010). Behavioural relevance of variation in white matter microstructure. Curr Opin Neurol 23:351–358.

McCulloch, W. S. (1944). The functional organization of the cerebral cortex. Physiol Rev 24:390-407.

Mountcastle, V. B. (1997). The columnar organization of the neocortex. Brain 120:701-722.

Pandit, A. S., Expert, P., Lambiotte, R., Bonnelle, V., Leech, R., Turkheimer, F. E., & Sharp, D. J. (2013). Traumatic brain injury impairs small-world topology. Neurology 80:1826-1833.

Park, H. J., & Friston, K. (2013). Structural and functional brain networks: from connections to cognition. Science 342:1238411.

Rubinov, M., & Sporns, O. (2010). Complex network measures of brain connectivity: uses and interpretations. Neuroimage 52:1059-1069.

Sutton, R. S., & Barto, A. G. (1998). Introduction to reinforcement learning (Vol. 135). Cambridge: MIT press.

Tang, E., Giusti, C., Baum, G. L., Gu, S., Pollock, E., Kahn, A. E., ... & Gur, R. E. (2017). Developmental increases in white matter network controllability support a growing diversity of brain dynamics. Nat Commun 8:1252.

Verstynen, T. D. (2015). How form constrains function in the human brain. Emerging Trends in the Social and Behavioral Sciences: An Interdisciplinary, Searchable, and Linkable Resource: 1-16.

Vettel, J. M., Cooper, N., Garcia, J. O., Yeh, F. C., & Verstynen, T. D. (2001). White Matter Tractography and Diffusion-Weighted Imaging. eLS, 1-9.

Vlooswijk, M. C. G., Vaessen, M. J., Jansen, J. F. A., de Krom, M. C. F. T. M., Majoie, H. J. M., Hofman, P. A. M., ... & Backes, W. H. (2011). Loss of network efficiency associated with cognitive decline in chronic epilepsy. Neurology 77: 938-944.

Watts, D. J., & Strogatz, S. H. (1998). Collective dynamics of 'small-world' networks. Nature 393:440.

Yeh, F. C., & Tseng, W. Y. I. (2011). NTU-90: a high angular resolution brain atlas constructed by q-space diffeomorphic reconstruction. Neuroimage 58:91-99.

Yeh, F. C., Verstynen, T. D., Wang, Y., Fernández-Miranda, J. C., & Tseng, W. Y. I. (2013). Deterministic diffusion fiber tracking improved by quantitative anisotropy. PloS One 8:e80713.

Yeh, F. C., Vettel, J. M., Singh, A., Poczos, B., Grafton, S. T., Erickson, K. I., ... & Verstynen, T. D. (2016). Quantifying differences and similarities in whole-brain white matter architecture using local connectome fingerprints. PLoS Comput Biol 12:e1005203.